

Heat-capacity measurements under uniaxial pressure using a piezo-driven device

Cite as: Rev. Sci. Instrum. **91**, 103903 (2020); <https://doi.org/10.1063/5.0021919>

Submitted: 15 July 2020 . Accepted: 07 October 2020 . Published Online: 21 October 2020

Y.-S. Li, R. Borth,  C. W. Hicks,  A. P. Mackenzie, and  M. Nicklas



View Online



Export Citation



CrossMark

ARTICLES YOU MAY BE INTERESTED IN

[Piezoelectric-driven uniaxial pressure cell for muon spin relaxation and neutron scattering experiments](#)



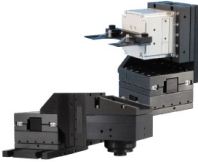
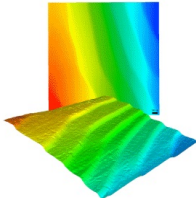
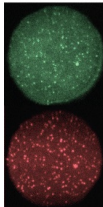
Review of Scientific Instruments **91**, 103902 (2020); <https://doi.org/10.1063/5.0025307>

[Polymerase chain reaction thermal cycling using the programmed tilt displacements of capillary tubes](#)

Review of Scientific Instruments **91**, 104105 (2020); <https://doi.org/10.1063/5.0007879>

[P Spice modeling of the pulsed electroacoustic method for dispersive polymer sample application](#)

Review of Scientific Instruments **91**, 105112 (2020); <https://doi.org/10.1063/5.0009706>

 MCL MAD CITY LABS INC. www.madcitylabs.com	<p>Nanopositioning Systems</p> 	<p>Modular Motion Control</p> 	<p>AFM and NSOM Instruments</p> 	<p>Single Molecule Microscopes</p> 
---	--	--	---	--



Heat-capacity measurements under uniaxial pressure using a piezo-driven device

Cite as: *Rev. Sci. Instrum.* **91**, 103903 (2020); doi: [10.1063/5.0021919](https://doi.org/10.1063/5.0021919)

Submitted: 15 July 2020 • Accepted: 7 October 2020 •

Published Online: 21 October 2020



View Online



Export Citation



CrossMark

Y.-S. Li,^{1,2} R. Borth,¹ C. W. Hicks,^{1,3}  A. P. Mackenzie,^{1,2}  and M. Nicklas^{1,a)} 

AFFILIATIONS

¹Max Planck Institute for Chemical Physics of Solids, Nöthnitzer Str. 40, 01187 Dresden, Germany

²Scottish Universities Physics Alliance (SUPA), School of Physics and Astronomy, University of St Andrews, St Andrews KY16 9SS, United Kingdom

³School of Physics and Astronomy, University of Birmingham, Birmingham B15 2TT, United Kingdom

^{a)}Author to whom correspondence should be addressed: Michael.Nicklas@cpfs.mpg.de

ABSTRACT

We report the development of a technique to measure heat capacity at large uniaxial pressure using a piezoelectric-driven device generating compressive and tensile strain in the sample. Our setup is optimized for temperatures ranging from 8 K down to millikelvin. Using an AC heat-capacity technique, we are able to achieve an extremely high resolution and to probe a homogeneously strained part of the sample. We demonstrate the capabilities of our setup on the unconventional superconductor Sr_2RuO_4 . By replacing thermometer and adjusting the remaining setup accordingly, the temperature regime of the experiment can be adapted to other temperature ranges of interest.

© 2020 Author(s). All article content, except where otherwise noted, is licensed under a Creative Commons Attribution (CC BY) license (<http://creativecommons.org/licenses/by/4.0/>). <https://doi.org/10.1063/5.0021919>

I. INTRODUCTION

Application of external pressure is a powerful method to tune the intricate interplay of competing energy scales in correlated materials and the emergence of novel unconventional phases in a clean fashion. It offers significant advantages as a control parameter compared with chemical substitution and application of magnetic fields because it does not introduce additional disorder as in the case of substitution of one element by the other one or polarize the electrons as a magnetic field does.

A large variety of experimental setups has been developed to probe physical properties under hydrostatic pressure.¹ In contrast, experiments under uniaxial pressure appeared to be limited to low pressure and only few experimental probes. Recently, however, the development of piezoelectric-driven pressure devices opened a new perspective.^{2,3} These devices allow the application of large positive and negative pressures, and the amplitude of the applied pressure can be easily changed at low temperatures. In a short period of time, experimental stages to access a large number of physical properties of materials have been developed. These include electrical transport,^{4,5} magnetic susceptibility,⁶ nuclear-magnetic resonance,^{7–9} muon-spin resonance,¹⁰ and angle-resolved photo

emission, for which mechanically or thermally activated cells have also been introduced.^{11–15}

An important quantity to characterize a material is the specific heat, which is the fundamental thermodynamic property giving information on the internal degrees of freedom of a material and the entropy related with them. To address the experimental challenge of studying the heat capacity under large uniaxial pressures, we employ a variation of known AC heat-capacity measurement techniques.¹⁶ Heat capacity measurement has been combined with uniaxial pressure previously,^{17–21} but with traditional, anvil-based uniaxial pressure cells. Samples have been thermally isolated by using low thermal conductivity materials, such as stainless steel or superconducting NbTi, as piston or additional spacer. However, in previous anvil-based uniaxial-pressure measurements, e.g., on the unconventional superconductor Sr_2RuO_4 , it did not prove practical to maintain high stress homogeneity,^{22,23} which is one of the main challenges in carrying out this kind of experiments. Furthermore, under applied uniaxial pressure, the samples even may deform plastically. To reduce these effects, we apply force to the sample through a layer of epoxy,² which acts as a conformal layer that dramatically improves stress homogeneity. However, it also makes heat-capacity measurement more challenging because the epoxy

layer provides an unavoidable strong thermal link to the pressure cell.

For our study, we have used Sr_2RuO_4 that provides a demanding test of our new apparatus. Sr_2RuO_4 is an unconventional superconductor with a superconducting transition temperature up to $T_c = 1.5$ K in the best crystals.^{24–26} From resistivity and magnetic susceptibility experiments, it is known that T_c shows a pronounced dependence on the applied uniaxial pressure.^{5,6,27} This and the sharp superconducting transition anomaly make it an ideal material to demonstrate the potential of our technique for the study of correlated materials. A successful experiment on Sr_2RuO_4 can only be done using a technique that introduces no disorder or plastic deformations and that probes a region in which the strain induced in the sample is highly homogeneous.

II. METHOD

For a setup in which the sample is strongly coupled to the environment as it is in a pressure cell, whether hydrostatic or uniaxial, standard quasi-adiabatic or relaxation techniques are limited to cases where the heat capacity of the whole pressure cell including the sample is measured and the heat capacity of the sample can then be separated from the (large) addenda. This implies restrictions on the materials that can be investigated and limits experiments to low temperatures. The advantage of such a technique is that one obtains absolute values of the heat capacity, but the resolution and the pressure regime are limited. In heat-capacity measurements at higher pressure, where anvil-type cells are used, or for uniaxial pressure experiments, the application of this technique is not possible anymore. The mass of sample is negligible with respect to that of the pressure apparatus. In these cases, the heat capacity can only be determined using an AC heat capacity measurement technique.¹⁶ With the AC technique, it is possible to record heat capacity data in a wide range of parameter space on a sample, which is not well thermally isolated from its environment by adjusting the measurement frequency. The drawback is that it is generally challenging to obtain absolute values of the heat capacity, and one usually has to be content with data having arbitrary units. As we demonstrate, however, it can still yield a wealth of useful information.

A. AC heat capacity

In the AC heat capacity measurement technique, an alternating current is applied at frequency $\omega/2$ to the heater, leading to an AC heat power at frequency ω to determine the heat capacity C_{AC} . Here, $\omega = 2\pi f$ is the angular frequency. The governing relationship for measurements of the AC heat capacity is

$$C_{AC} = \frac{P}{\omega T_{AC}} F(\omega). \quad (1)$$

Here, P is the average power and $F(\omega)$ is a frequency response curve that characterizes the thermalization of the sample and differs from sample to sample because it depends on time constants determined by thermal conductances and heat capacities of the system. $F(\omega)$ depends on the time constants τ_1 and τ_2 ,

$$F(\omega) = \left[1 + \frac{1}{\omega^2 \tau_1^2} + \omega^2 \tau_2^2 \right]^{-1/2}. \quad (2)$$

$\tau_1 = C_{AC}/k_b$ describes the time scale of the applied heat power decaying to the environment, whereas $\tau_2 = \sqrt{\tau_h^2 + \tau_\theta^2 + \tau_{\text{int}}^2}$ describes the internal thermal time scale within the system itself. Here, $\tau_h = C_h/k_h$, $\tau_\theta = C_\theta/k_\theta$ and $\tau_{\text{int}} = C_s/k_s$ [see also Fig. 1(a)]. The time constants τ_h , τ_θ , and τ_{int} describe the time scales for the heater and thermometer and sample to be thermalized, respectively. C_h , C_θ , and C_s are the heat capacity of the heater, thermometer, and sample, respectively. For a good design, the responses of heater and thermometer need to be fast, so one should aim at $\tau_{\text{int}} \gg \tau_h$ and τ_θ .

A schematic diagram of $F(\omega)$ is shown in Fig. 1(b). At low frequencies, indicated as regime I, $\omega \ll \omega_1 = 1/\tau_1 = k_b/C_{AC}$, $F(\omega)$ is reduced due to dissipation of temperature oscillations into the environment and at high frequencies, $\omega \gg \omega_2 = 1/\tau_2 \cong k_s/C_s$, because the heater-sample-temperature sensor system does not thermalize, marked as regime III. In the plateau region between these limits, $F(\omega) \approx 1$ and

$$C_{AC} \approx \frac{P}{\omega T_{AC}}. \quad (3)$$

In addition to the temperature oscillations, the application of the oscillatory heating power leads to a temperature offset T_{DC} in the sample, which can be determined in the low frequency limit

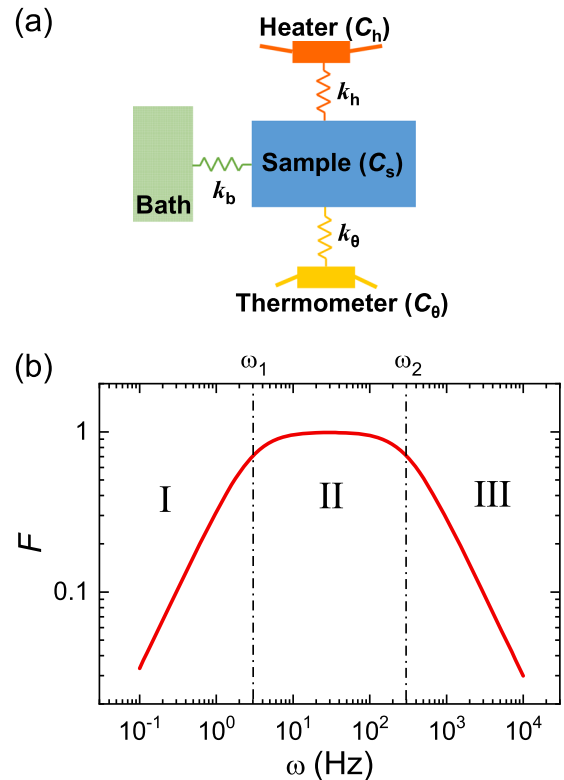


FIG. 1. (a) Schematic drawing of the thermal couplings of a sample in an AC heat-capacity setup. (b) A schematic diagram of the frequency response curve F against ω . ω is the angular frequency of the temperature oscillation. The curve can be divided into three regions separated by ω_1 and ω_2 .

$\omega \ll \omega_1$. Here, $F(\omega) = \omega\tau_1$ and the temperature offset can be estimated as

$$T_{DC} \approx \frac{P}{k_b}. \quad (4)$$

B. Experimental setup

The general considerations in the section above show that it should be possible to measure the heat capacity in an uniaxial pressure apparatus, as shown in Fig. 2(a), by choosing the correct set of experimental parameters. In the following, we will explain the experimental setup and describe the details of the preparation process using the example of a Sr_2RuO_4 single crystal.

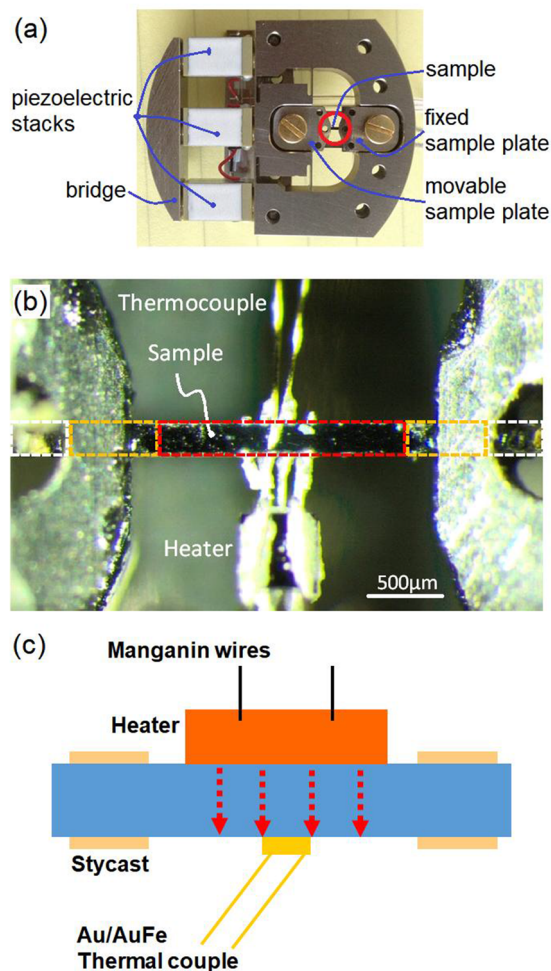


FIG. 2. (a) Photograph of the uniaxial pressure apparatus used in the present study. The red circle marks the sample region. (b) Photograph of the setup of the heat capacity measurements under strain including the heater and thermocouple. The sample is glued between the jaws of the uniaxial pressure device. The exposed length, width, and thickness of the shown sample are 2 mm, 200 μm , and 150 μm , respectively. The device allows the application of compressive and tensile strains. The red, yellow, and white rectangles represent the (quasi)homogeneous, inhomogeneous, and unstrained regions, respectively (see the text for details). (c) Schematic diagram of the setup illustrating the photograph in (b).

The sample is marked by a red circle in Fig. 2(a) and shown in detail in Fig. 2(b). In this setup, the applied force results in a normal strain

$$\varepsilon_{xx} = \frac{l - l_0}{l_0} \quad (5)$$

in the sample. Here, l_0 is the length of the unstrained sample and l is the length of the strained sample. The length change is measured capacitively and can be controlled. The applied strain can go beyond 1%. In Sr_2RuO_4 , the Young's modulus is about 180 GPa, and correspondingly, the applied uniaxial pressure can reliably reach up to about 2 GPa. However, the maximum uniaxial pressure depends strongly on the mechanical properties of the investigated material. Further details can be found in Ref. 2. The present AC heat-capacity technique can be adapted to different types of uniaxial pressure devices, e.g., to a stress-controlled apparatus,³ and is fully compatible with experiments in magnetic fields.

In Fig. 2(b), we show a photograph of the bar-shaped sample that has been carefully cut, polished, and then mounted within the jaws of the uniaxial pressure rig. The nature of the apparatus means that only the central part of the sample is homogeneously strained. Force is transferred to the sample through the epoxy layer around the sample. The sample ends that are protruding beyond it are unstrained, and there are intermediate regions, marked in yellow in Fig. 2(b), where the strain is built up. Therefore, we have to choose the measurement conditions in a way that we only probe the homogeneous part of the sample. In the example of a Sr_2RuO_4 single crystal, we will demonstrate that this is, in principle, possible by varying the excitation frequency $f_{\text{exc}} = f/2$ of the heater, if the characteristic parameters of the setup, such as the different thermal conductances, have been chosen in the appropriate range.

For the experiments, single crystalline Sr_2RuO_4 was aligned using a bespoke Laue x-ray camera and cut using a wire saw into thin bars with whose long axis aligned with the [100] direction of the crystal. For the best results, these bars were polished using homemade apparatus based on diamond impregnated paper with a minimum grit size of 1 μm . The bar was then mounted within the jaws of the uniaxial pressure rig using Stycast 2850FT epoxy with Catalyst 23LV (Henkel Loctide). A resistive thin film resistor chip (State of the Art, Inc., Series No.: S0202DS1001FKW) as heater and a Au-AuFe(0.07%) thermocouple are fixed to opposite sides of the sample using Dupont 6838 single component silver-filled epoxy. The resistance of heater is about 640 Ω , and the applied power is in the range of μW . The heater is connected electrically using manganin wires, providing a low thermal conductance to the bath. At 1 K, the thermal conductance of the Stycast layers and the manganin wires is about 10^{-4} W/K and 10^{-7} W/K, respectively. Thus, the heat loss is largely dominated by the Stycast layers. The thermocouple was spot-welded in-house, and its calibration is fixed by reference to that of a calibrated RuO_2 thermometer.²⁸ Special care was taken when epoxying to the pressure cell to minimize tilt and ensure an as homogeneous strain field as possible.

The uniaxial pressure apparatus was mounted on a dilution refrigerator (Oxford Instruments), with thermal coupling to the mixing chamber via a high purity silver wire. The data were acquired between 500 mK and 4.2 K, with operation above 1.5 K achieved by circulating a small fraction of the mixture. The extremely low noise level of 20 pV/ $\sqrt{\text{Hz}}$ on the thermocouple readout was achieved by the combination of an EG&G 7265 lock-in amplifier and a high

frequency low temperature transformer (LTT-h from CMR direct) mounted on the 1 K pot of the dilution refrigerator, operating at a gain of 300. The input impedance of the transformer is about 0.1Ω , which ensured a flat frequency response from several hundred Hz to several tens of kHz. A Keithley 6221 low-noise current source was used to drive the heater. The piezo-electric actuators were driven at up to ± 400 V using a bespoke high-voltage amplifier.

C. Strain inhomogeneity

The nature of our setup is that the strain profile along the direction of the application of the uniaxial pressure is not homogeneous. As we will describe below, by adjusting the excitation frequency f_{exc} to an appropriate value, the actual heat-capacity measurement can be confined to the quasi-homogeneously strained region of the sample. Besides this source of strain inhomogeneity, there are other sources that can be reduced in the preparation and mounting process of the sample in the apparatus.

1. Imperfections of sample surface and geometry

The bar-shaped needles cut from crystals have terraces and irregular shapes on their surface, which can induce inhomogeneous strain fields when they are under uniaxial pressure. Imperfections may also lead to an early failure of pressurized samples reducing the maximum achievable pressure. A perfect sample is a cuboid, i.e., each surface is parallel to the opposite one, and has a smooth surface roughness. Therefore, we carefully polish our samples and inspect the shape and the surface quality under a microscope before mounting on the uniaxial pressure apparatus.

2. Bending

Asymmetric mounting of a sample leads to bending.²⁹ An ideal sample mounting is a sample mounted between two plates with symmetrical epoxy layers on the top and at the bottom. However, the sample might end up with a small offset in height. To reduce inhomogeneity in preparing the sample, we aim for an aspect ratio $l_s/t > 10$, where l_s is the exposed length and t is the thickness of the sample.

3. Mounting of the heater

One of the main sources of inhomogeneous strain fields originates from the sample configuration in the AC heat-capacity setup. In order to transmit the heating power from the heater resistance to the sample, we use thermal contacts made by silver wires glued to the sample using silver-filled epoxy. Since the Young's modulus of silver and the sample are generally very different, as in our example of Sr_2RuO_4 , the contacts create inhomogeneous strain fields. We tried to minimize this effect. We realized two different types of silver contacts to the sample. Figures 3(a) and 3(c) show photographs of the setups. In the first one, a silver strip was glued on a contact length of about $300 \mu\text{m}$ on both edges to the sample using silver-filled epoxy. In the second, the thermal contact is divided into 4 smaller areas instead of a large one by gluing eight silver wires with diameter of $50 \mu\text{m}$ on both edges. The total contact area in both cases is almost the same. The experiments on our test sample Sr_2RuO_4 showed indeed a significant sharpening of the superconducting transition anomaly in the latter case.

In addition to the experiments, we simulated the strain fields in the sample by a finite element method using a commercial

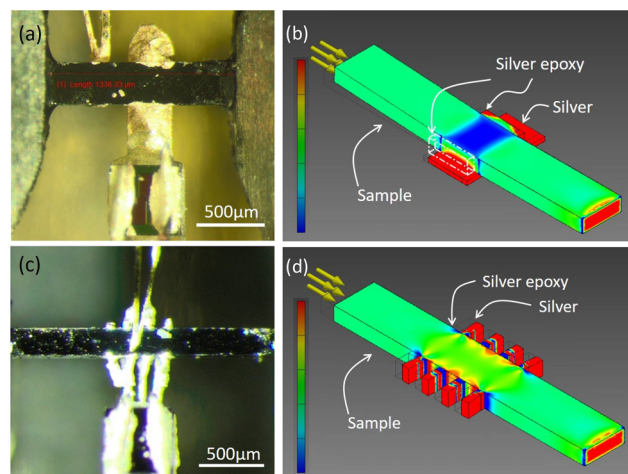


FIG. 3. (a) Heater fixed with a silver foil to the sample. The contact to the sample is on the whole plane. The exposed length, width, and thickness of the shown sample are $l = 1.3$ mm, $w = 300 \mu\text{m}$, and $t = 100 \mu\text{m}$. (b) The simulation of the strain ϵ_{xx} pattern corresponding to the setup in (a). One of the silver-filled epoxy blocks is set to be invisible, as indicated by the dashed-dotted lines, such that the strain profile on the edge of the sample is visible. (c) Heater fixed to the sample by four thin silver wires on the edges of the sample. The sample dimensions are $l = 2$ mm, $w = 200 \mu\text{m}$, and $t = 150 \mu\text{m}$. (d) Corresponding simulation to (c). The strain inhomogeneity is reduced in the center compared with the setup shown in (a). In the case of the two simulations, the same dimensions, $l = 2$ mm, $w = 300 \mu\text{m}$, and $t = 100 \mu\text{m}$, have been used.

software package.³⁰ For the simulation, we set the Young's modulus of the sample to 180 GPa and Poisson's ratio to 0.33. For the dimensions of the sample, we used a thickness $100 \mu\text{m}$, width $300 \mu\text{m}$, and length 2 mm. One of the sample ends was set to be fixed and the other end was subjected to a pressure of 0.18 GPa, leading to $\epsilon_{xx} = 0.1\%$. The silver and silver-filled epoxy were set to have Poisson's ratio of 0.35. Young's modulus for the silver epoxy was set to be 1/3 of that of the silver, which is 110 GPa. The results for both configurations are shown in Figs. 3(b) and 3(d). The color bar shows the strain scale ranging from 0.07% to 0.13%. In the first configuration, with silver strip glued with silver-filled epoxy on both edges to the sample, the strain inhomogeneity on the sample is greater than 60% at the center [see Fig. 3(b)]. In the second design using eight silver wires with diameter of $50 \mu\text{m}$ on both edges for the thermal contact, the strain inhomogeneity is strongly reduced in the bulk, except in the regions very close to the contact surfaces. Since heat capacity is a bulk-sensitive measurement, the inhomogeneity near the surface is negligible. The strain inhomogeneity in this configuration is only about 10% in the center region of the sample. This shows that it is highly desirable to have separated smaller contact areas to transmit the heat to the sample in order to reduce strain inhomogeneities in accordance with the experimental results. In the following, we continued with the second configuration.

III. RESULTS

We demonstrate the capabilities of our setup and discuss its advantages and limitations by showing representative data from experiments on Sr_2RuO_4 . The first step in an AC heat-capacity experiment is to find a suitable measurement frequency in the

plateau region of the frequency response curve $F(\omega)$. We note that the existence of this plateau depends on the respective characteristics of the setup, as discussed in Sec. II A. If a suitable frequency has been found, temperature sweeps, also in applied magnetic field, or pressure/magnetic field ramps can be conducted, and the heat capacity is recorded. According to Eq. (3), we will plot our results on Sr_2RuO_4 as $P/[\omega T_{AC}(T)]$. As we will discuss in Sec. III C, $C_{AC} \approx P/(\omega T_{AC})$ is not strictly valid in our setup and has to be treated with caution.

A. Measuring frequency

Figure 4(a) shows the frequency response at 1 K and 4.23 K in the case of our example Sr_2RuO_4 crystal. It shows a broad plateau between a few hundred hertz and several kilohertz at both temperatures, attesting that in principle, heat-capacity measurements should be possible in the desired temperature range. By raising the temperature from 1 K to 4.23 K, the plateau narrows slightly but remains well-defined.

In the lower frequency part of the plateau in Fig. 4(a), temperature oscillations extend throughout the sample, and all three regions, the homogeneously strained at the center, the unstrained portions at the ends, and the regions where strain builds up, are probed in a measurement [see Fig. 2(b)]. Figure 4(b) shows $P/[\omega T_{AC}(T)]$ recorded at $f_{exc} = 313$ Hz for different ϵ_{xx} . At zero strain, we see a single sharp transition anomaly at $T_c \approx 1.45$ K. Upon increasing $|\epsilon_{xx}|$, the step-like feature moves to higher temperatures, consistent with the increase in T_c with strain,⁶ but a second feature remains at the original zero-strain transition. This latter feature stems from the unstrained part of the sample.

To reduce the size of the probed part of the sample and restrict it to the homogeneously strained region at the center, we increased the measurement frequency. We note that we still stay in the plateau region of frequency response curve. To demonstrate the importance of this increase in measurement frequency, we applied modest strain $\epsilon_{xx} = -0.19\%$ and increased f_{exc} from 313 Hz in steps to 2503 Hz. The data are displayed in Fig. 4(c). At 313 Hz and 613 Hz, in addition to the peak at ≈ 1.65 K corresponding to the transition at the central strained portion of the sample, a smaller peak is visible at ≈ 1.45 K, corresponding to the transition in the end portions. This feature shows that temperature oscillations extend into the sample ends at these frequencies. To avoid this, one has to work at the high end of the feasible range of frequencies. For this particular sample, a measurement frequency above ~ 1.5 kHz was required. Working at high frequencies with low enough power to avoid heating gives a very small signal, an rms thermocouple voltage of only 1 nV–2 nV. Therefore, the described low temperature passive amplification was employed to achieve an rms noise level of $20 \text{ pVHz}^{-1/2}$, ensuring a signal-to-noise ratio in excess of 50.

B. Heat-capacity results on Sr_2RuO_4

Based on considerations outlined in Sec. III A, we selected an excitation frequency of $f_{exc} = 1503$ Hz to measure the heat capacity of Sr_2RuO_4 . The results for three different strains $\epsilon_{xx} = 0\%$, -0.25% , and -0.37% are presented in Fig. 5 as $P/[\omega T_{AC}(T)]$. Additionally, the inset shows the results from a standard relaxation-type heat-capacity measurement from a piece of sample cut from the same crystal. It is qualitatively similar to the results in the uniaxial pressure cell at zero strain.

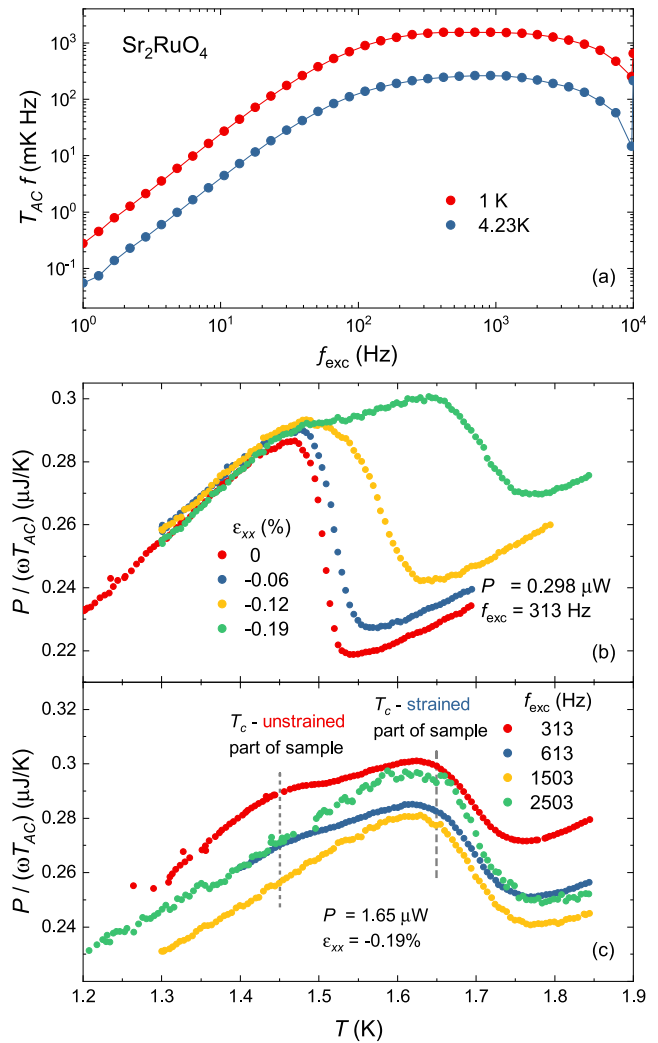


FIG. 4. (a) Frequency sweeps at 1 K and 4.23 K. (b) Data recorded at 313 Hz for zero and small strains up to $\epsilon_{xx} = -0.19\%$. (c) Data on Sr_2RuO_4 in the region around its superconducting transition at $\epsilon_{xx} = -0.19\%$ for different frequencies.

According to Eq. (3), we find $C_{AC}(T) \approx P/[\omega T_{AC}(T)]$. However, this relation has to be taken with caution since the probed sample volume is not constant as a function of temperature. We have selected f_{exc} in order to probe the homogeneously strained portion of the sample, but we have to notice that the thermal conductivity κ of any studied material varies as a function of temperature and strain, and as a consequence, the probed sample volume also changes. To obtain absolute values of the volume specific heat $c_v(T)$ at a certain strain, the temperature dependence of the thermal conductivity $\kappa(T)$ has to be known at that strain too.

C. Determination of the volume specific heat

The conversion between the measured signal and the volume or molar specific heat is trivial in a conventional setup because the volume (or mass) of the sample is constant. In our measurements,

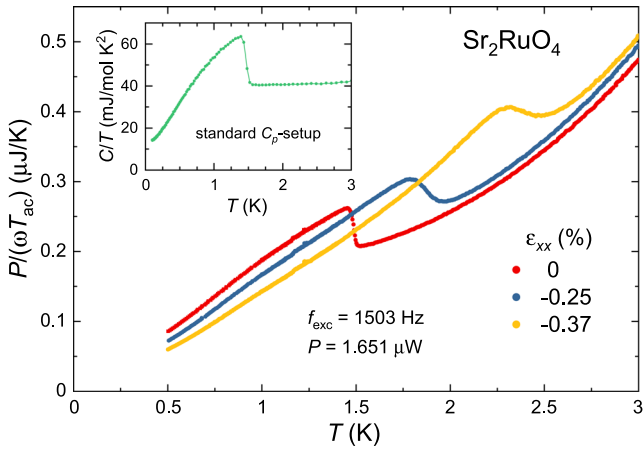


FIG. 5. Recorded signal $P/[\omega T_{AC}(T)]$ of Sr_2RuO_4 as a function of temperature for three different strains: $\epsilon_{xx} = 0\%$, -0.25% , and -0.37% . The inset shows a specific-heat experiment on a piece from the same crystal using a standard relaxation time method.

the probed sample volume varies since the thermal diffusion length l_d , which depends on thermal conductivity, specific heat, and frequency, changes as a function of temperature. Therefore, it is non-trivial to convert our data $P/[\omega T_{AC}(T)]$ to volume specific heat c_v . We start with an ideal case to demonstrate the relation between $P/[\omega T_{AC}(T)]$ and c_v in the case of our experimental setup. Suppose that the heater contact is point-like at the center of a very narrow sample such that the heat flow is one-dimensional propagating in the left and right directions. The probed volume V is equal to the cross-sectional area A times twice the diffusion length l_d , which is a function of the angular frequency ω , the volume specific heat c_v , and the thermal conductivity κ ,

$$l_d = \sqrt{\frac{2\kappa(T)}{\omega c_v(T)}}, \quad (6)$$

where C_{AC} can be expressed as follows:

$$C_{AC} = c_v \times V = c_v \times A \times l_d = \frac{2A}{\sqrt{\omega}} \sqrt{2\kappa(T)c_v(T)}. \quad (7)$$

By using Eqs. (1) and (7), we finally obtain the volume specific heat c_v

$$c_v(T) = \left(\frac{P \times F(\omega)}{2A}\right)^2 \times \frac{1}{\omega \times 2\kappa(T)} \times \frac{1}{[T_{AC}(T)]^2}. \quad (8)$$

This exemplifies the reciprocal dependence of $c_v(T)$ on the thermal conductivity and the square of the temperature-oscillation amplitude in the case of a simplified one-dimensional model.

We further note that the excitation frequency in our current measurement is not too far away from the upper cut-off frequency, which describes the time scale for the heat propagating from the heater to the thermocouple. At this excitation frequency, $F(\omega) < 1$ and depends on temperature adding a further uncertainty on the determination of $c_v(T)$.

The validity of Eqs. (7) and (8) is based on the above-mentioned assumptions that the heater contact is point-like and the heat flow is one-dimensional. In reality, both the sample width and the heater

contact size are finite. This implies that for the experimental setup to satisfy the assumptions of the examined model system, the exposed sample length (l_s) must be far longer than the heater length (l_h) and the sample width (w_s), $l_s \gg l_h, w_s$. Our present setup is already a good approximation to an ideal configuration but could, in principle, be further optimized.

Despite the above caveats, we note that in some cases, quantitative statements on the evolution of the specific heat on varying uniaxial pressure are possible based on the presently accessible data. For example, in superconductors, as in the case of Sr_2RuO_4 , it is possible to obtain information on the evolution of the size of the superconducting transition anomaly with pressure, which is an important quantity characterizing superconductivity. In that case, the thermal conductivity does not show any abrupt change across the transition and close to T_c ,

$$\frac{c_v^s}{c_v^n} = \frac{\kappa_n}{\kappa_s} \times \left(\frac{T_{AC}^n}{T_{AC}^s}\right)^2 \approx \left(\frac{T_{AC}^n}{T_{AC}^s}\right)^2 \quad (9)$$

with $\kappa_n \approx \kappa_s$. The indices s and n indicate the corresponding values in the superconducting and the normal states, respectively.

IV. CONCLUSION

We have developed a new experimental setup using piezoelectric-driven uniaxial pressure cells for probing heat capacity at low temperatures. By optimizing our preparation and measuring processes, we achieve an extremely high resolution and a high strain homogeneity in the probed sample volume. The technique can be easily extended to different temperature regions. In addition to temperature sweeps, heat capacity can be recorded as a function of applied pressure, and our apparatus is also fully compatible with work in magnetic fields.

ACKNOWLEDGMENTS

The authors thank A. S. Gibbs, F. Jerzembeck, N. Kikugawa, Y. Maeno, and D. A. Sokolov for providing and characterizing the samples and M. Brando and U. Stockert for experimental support. Y.S.L. acknowledges the support of a St Leonards scholarship from the University of St Andrews, the Engineering and Physical Sciences Research Council via the Scottish Condensed Matter Centre for Doctoral Training under Grant No. EP/G03673X/1, and the Max Planck Society.

DATA AVAILABILITY

The data that support the findings of this study are available from the corresponding author upon reasonable request.

REFERENCES

- ¹M. Nicklas, "Pressure probes," in *Strongly Correlated Systems: Experimental Techniques*, edited by A. Avella and F. Mancini (Springer Berlin Heidelberg, Berlin, Heidelberg, 2015), pp. 173–204.
- ²C. W. Hicks, M. E. Barber, S. D. Edkins, D. O. Brodsky, and A. P. Mackenzie, "Piezoelectric-based apparatus for strain tuning," *Rev. Sci. Instrum.* **85**, 065003 (2014).
- ³M. E. Barber, A. Steppe, A. P. Mackenzie, and C. W. Hicks, "Piezoelectric-based uniaxial pressure cell with integrated force and displacement sensors," *Rev. Sci. Instrum.* **90**, 023904 (2019).

- ⁴A. Stern, M. Dzero, V. M. Galitski, Z. Fisk, and J. Xia, "Surface-dominated conduction up to 240 K in the Kondo insulator SmB_6 under strain," *Nat. Mater.* **16**, 708–711 (2017).
- ⁵A. Steppke, L. Zhao, M. E. Barber, T. Scaffidi, F. Jerzembeck, H. Rosner, A. S. Gibbs, Y. Maeno, S. H. Simon, A. P. Mackenzie, and C. W. Hicks, "Strong peak in T_c of Sr_2RuO_4 under uniaxial pressure," *Science* **355**, eaaf9398 (2017).
- ⁶C. W. Hicks, D. O. Brodsky, E. A. Yelland, A. S. Gibbs, J. A. N. Bruin, M. E. Barber, S. D. Edkins, K. Nishimura, S. Yonezawa, Y. Maeno, and A. P. Mackenzie, "Strong increase of T_c of Sr_2RuO_4 under both tensile and compressive strain," *Science* **344**, 283–285 (2014).
- ⁷T. Kissikov, R. Sarkar, B. T. Bush, M. Lawson, P. C. Canfield, and N. J. Curro, "Piezoelectric-based uniaxial pressure cell with integrated force and displacement sensors," *Rev. Sci. Instrum.* **88**, 103902 (2017).
- ⁸Y. Luo, A. Pustogov, P. Guzman, A. P. Dioguardi, S. M. Thomas, F. Ronning, N. Kikugawa, D. A. Sokolov, F. Jerzembeck, A. P. Mackenzie, C. W. Hicks, E. D. Bauer, I. I. Mazin, and S. E. Brown, "Normal state ^{17}O NMR studies of Sr_2RuO_4 under uniaxial stress," *Phys. Rev. X* **9**, 021044 (2019).
- ⁹A. Pustogov, Y. Luo, A. Chronister, Y.-S. Su, D. A. Sokolov, F. Jerzembeck, A. P. Mackenzie, C. W. Hicks, N. Kikugawa, S. Raghu, E. D. Bauer, and S. E. Brown, "Constraints on the superconducting order parameter in Sr_2RuO_4 from oxygen- 17 nuclear magnetic resonance," *Nature* **574**, 72–75 (2019).
- ¹⁰V. Grinenko, S. Ghosh, R. Sarkar, J.-C. Orain, A. Nikitin, M. Elender, D. Das, Z. Guguchia, F. Brückner, M. E. Barber, J. Park, N. Kikugawa, D. A. Sokolov, J. S. Bobowski, T. Miyoshi, Y. Maeno, A. P. Mackenzie, H. Luetkens, C. W. Hicks, and H.-H. Klauss, "Split superconducting and time-reversal symmetry-breaking transitions, and magnetic order in Sr_2RuO_4 under uniaxial stress," *arXiv* **2001.08152** (2020).
- ¹¹D. Flötotto, Y. Bai, Y.-H. Chan, P. Chen, X. Wang, P. Rossi, C.-Z. Xu, C. Zhang, J. A. Hlevyack, J. D. Denlinger, H. Hong, M.-Y. Chou, E. J. Mittemeijer, J. N. Eckstein, and T.-C. Chiang, "In situ strain tuning of the Dirac surface states in Bi_2Se_3 films," *Nano Lett.* **18**, 5628–5632 (2018).
- ¹²S. Riccò, M. Kim, A. Tamai, S. McKeown Walker, F. Y. Bruno, I. Cucchi, E. Cappelli, C. Besnard, T. K. Kim, P. Dudin, M. Hoesch, M. J. Gutmann, A. Georges, R. S. Perry, and F. Baumberger, "In situ strain tuning of the metal-insulator-transition of Ca_2RuO_4 in angle-resolved photoemission experiments," *Nat. Commun.* **9**, 4535 (2018).
- ¹³H. Pfau, S. D. Chen, M. Yi, M. Hashimoto, C. R. Rotundu, J. C. Palmstrom, T. Chen, P.-C. Dai, J. Straquadine, A. Hristov, R. J. Birgeneau, I. R. Fisher, D. Lu, and Z.-X. Shen, "Momentum dependence of the nematic order parameter in iron-based superconductors," *Phys. Rev. Lett.* **123**, 066402 (2019).
- ¹⁴H. Pfau, C. R. Rotundu, J. C. Palmstrom, S. D. Chen, M. Hashimoto, D. Lu, A. F. Kemper, I. R. Fisher, and Z.-X. Shen, "Detailed band structure of twinned and detwinned BaFe_2As_2 studied with angle-resolved photoemission spectroscopy," *Phys. Rev. B* **99**, 035118 (2019).
- ¹⁵V. Sunko, E. Abarca Morales, I. Marković, M. E. Barber, D. Milosavljević, F. Mazzola, D. A. Sokolov, N. Kikugawa, C. Cacho, P. Dudin, H. Rosner, C. W. Hicks, P. D. C. King, and A. P. Mackenzie, "Direct observation of a uniaxial stress-driven Lifshitz transition in Sr_2RuO_4 ," *npj Quantum Mater.* **4**, 46 (2019).
- ¹⁶P. F. Sullivan and G. Seidel, "Steady-state, ac-temperature calorimetry," *Phys. Rev.* **173**, 679 (1968).
- ¹⁷D. S. Jin, S. A. Carter, B. Ellman, T. F. Rosenbaum, and D. G. Hinks, "Uniaxial-stress anisotropy of the double superconducting transition in UPt_3 ," *Phys. Rev. Lett.* **68**, 1597–1600 (1992).
- ¹⁸P. H. P. Reinders, B. Wand, F. Steglich, G. Fraunberger, G. R. Stewart, and G. Adrian, "Specific-heat measurements on UBe_{13} under uniaxial pressure," *Europhys. Lett. (EPL)* **25**, 619–624 (1994).
- ¹⁹C. F. Miclea, F. M. Grosche, J. Sichelschmidt, G. R. Stewart, G. Sparn, and F. Steglich, "Unconventional superconductivity in UPt_3 probed by uniaxial stress," *Physica B* **312–313**, 97–99 (2002).
- ²⁰R. J. Zieve, R. Duke, and J. L. Smith, "Pressure and linear heat capacity in the superconducting state of thoriated UPt_3 ," *Phys. Rev. B* **69**, 144503 (2004).
- ²¹O. M. Dix, A. G. Swartz, R. J. Zieve, J. Cooley, T. R. Sayles, and M. B. Maple, "Anisotropic dependence of superconductivity on uniaxial pressure in CeIrIn_5 ," *Phys. Rev. Lett.* **102**, 197001 (2009).
- ²²S. Kittaka, H. Taniguchi, S. Yonezawa, H. Yaguchi, and Y. Maeno, "Pressure and linear heat capacity in the superconducting state of thoriated UPt_3 ," *Phys. Rev. B* **81**, 180510 (2010).
- ²³H. Taniguchi, K. Nishimura, S. K. Goh, S. Yonezawa, and Y. Maeno, "Unconventional strain dependence of superconductivity in spin-triplet superconductor Sr_2RuO_4 ," *J. Phys. Soc. Jpn.* **84**, 014707 (2015).
- ²⁴A. P. Mackenzie, R. K. W. Haselwimmer, A. W. Tyler, G. G. Lonzarich, Y. Mori, S. Nishizaki, and Y. Maeno, "Extremely strong dependence of superconductivity on disorder in Sr_2RuO_4 ," *Phys. Rev. Lett.* **80**, 161–164 (1998).
- ²⁵A. P. Mackenzie and Y. Maeno, "The superconductivity of Sr_2RuO_4 and the physics of spin-triplet pairing," *Rev. Mod. Phys.* **75**, 657–712 (2003).
- ²⁶A. P. Mackenzie, T. Scaffidi, C. W. Hicks, and Y. Maeno, "Even odder after twenty-three years: The superconducting order parameter puzzle of Sr_2RuO_4 ," *npj Quantum Mater.* **2**, 40 (2017).
- ²⁷M. E. Barber, A. S. Gibbs, Y. Maeno, A. P. Mackenzie, and C. W. Hicks, "Resistivity in the vicinity of a van Hove singularity: Sr_2RuO_4 under uniaxial pressure," *Phys. Rev. Lett.* **120**, 076602 (2018).
- ²⁸In the temperature range between 0.15 and 4.5 K, the thermopower S of the $\text{Au-AuFe}(0.07\%)$ thermocouple is described by $S(T) = [10.1483 \cdot T/K - 8.75772 \cdot (T/K)^2 + 4.00231 \cdot (T/K)^3 - 0.838741 \cdot (T/K)^4 + 0.0667604 \cdot (T/K)^5] \mu\text{V/K}$.
- ²⁹M. E. Barber, Ph.D. thesis, University of St. Andrews, 2017.
- ³⁰Autodesk Inventor 2015, Autodesk, Inc.